Benzo[1,2-b:4,5-b']dithiophene as a weak donor component for push-pull materials displaying thermally activated delayed fluorescence or room temperature phosphorescence

Cardeynaels, Tom; Paredis, Simon; Danos, Andrew; Vanderzande, Dirk; Monkman, Andrew P.; Champagne, Benoît; Maes, Wouter

Published in:
Dyes and pigments

DOI:
10.1016/j.dyepig.2020.109022

Publication date:
2021

Document Version
Publisher's PDF, also known as Version of record

Dyes and Pigments 186 (2021) 109022

Contents lists available at ScienceDirect

Dyes and Pigments

journal homepage: http://www.elsevier.com/locate/dyepig

Benzo[1,2-*b*:4,5-*b*']dithiophene as a weak donor component for push-pull materials displaying thermally activated delayed fluorescence or room temperature phosphorescence

Tom Cardeynaels [a,b], Simon Paredis [a], Andrew Danos [c], Dirk Vanderzande [a], Andrew P. Monkman [c], Benoît Champagne [b], Wouter Maes [a,*]

[a] Hasselt University, Institute for Materials Research (IMO-IMOMEC), Design & Synthesis of Organic Semiconductors (DSOS), Agoralaan 1, 3590 Diepenbeek, Belgium and IMOMEC Division, IMEC, Wetenschapspark 1, 3590, Diepenbeek, Belgium

[b] University of Namur, Laboratory of Theoretical Chemistry, Theoretical and Structural Physical Chemistry Unit, Namur Institute of Structured Matter, Rue de Bruxelles 61, 5000, Namur, Belgium

[c] OEM Group, Department of Physics, Durham University, South Road, Durham, DH1 3LE, United Kingdom

ARTICLE INFO

Keywords:
Thermally activated delayed fluorescence
Organic light-emitting diodes
Room temperature phosphorescence
Benzo[1,2-*b*:4,5-*b*']dithiophene
Photophysical and quantum-chemical characterizations

ABSTRACT

In the search for high-performance donor-acceptor type organic compounds displaying thermally activated delayed fluorescence (TADF), triisopropylsilyl-protected benzo[1,2-*b*:4,5-*b*']dithiophene (BDT-TIPS) is presented as a novel donor component in combination with two known acceptors: dimethyl-9*H*-thioxanthenedioxide (TXO2) and dibenzo[*a*,*c*]phenazinedicarbonitrile (CNQxP). For a broader comparison, the same acceptors are also combined with the well-studied 9,9-dimethyl-9,10-dihydroacridine (DMAC) donor. Optimized BDT-TIPS-containing structures show calculated dihedral angles of around 50° and well-separated highest occupied and lowest unoccupied molecular orbitals, although varying singlet-triplet energy gaps are observed experimentally. By changing the acceptor moiety and the resulting ordering of excited states, room temperature phosphorescence (RTP) attributed to localized BDT-TIPS emission is observed for TXO2-BDT-TIPS, whereas CNQxP-BDT-TIPS affords a combination of TADF and triplet-triplet annihilation (TTA) delayed emission. In contrast, strong and pure TADF is well-known for TXO2-DMAC, whereas CNQxP-DMAC shows a mixture of TADF and TTA at very long timescales. Overall, BDT-TIPS represents an alternative low-strength donor component for push-pull type TADF emitters that is also able to induce RTP properties.

1. Introduction

Organic light-emitting diodes (OLEDs) have proven to be a competitive replacement for older lighting technologies such as halogen lamps and inorganic LEDs, as well as display technologies such as liquid crystal displays (LCDs) [1–5]. Nevertheless, challenges remain toward cost-efficient, sustainable and low power-draw devices with a sufficiently long lifetime [1,3]. On the road to higher external quantum efficiencies (EQEs), a major step was taken by the introduction of heavy-metal-containing organic complexes, allowing phosphorescence from triplet excitons as an efficient emission pathway [6]. Intersystem crossing (ISC) from the singlet to the emissive triplet state allows the emitter to harvest all excitons through the phosphorescence channel, leading to internal quantum efficiencies (IQEs) of up to 100%. Although light out-coupling is still far from ideal and phosphorescence is an intrinsically spin-forbidden (and therefore slow) process, these phosphorescent OLEDs (PhOLEDs) are able to afford EQEs of 30% and above [5,7,8]. PhOLEDs have found their way to commercial applications such as OLED smartphone and television screens, but still suffer from two major drawbacks: a lack of stable blue emitters due to the relatively weak ligand-metal bonds, and reduced sustainability due to the presence of heavy-metal complexes.

Thermally activated delayed fluorescence (TADF) has the potential to overcome these issues, providing up to 100% IQE without the use of heavy-metal complexes [9,10]. In the TADF mechanism, the first excited singlet and triplet states have to be close in energy. The small singlet-triplet energy splitting (ΔE_{ST}) allows reverse intersystem crossing (rISC) of excitons from the non-emissive triplet to the singlet

* Corresponding author.
E-mail address: wouter.maes@uhasselt.be (W. Maes).

https://doi.org/10.1016/j.dyepig.2020.109022
Received 29 September 2020; Received in revised form 12 November 2020; Accepted 19 November 2020
Available online 28 November 2020

state [10]. In contrast to triplet emission in PhOLEDs, TADF emission therefore occurs exclusively through the singlet state. The rISC process is crucial to obtain high efficiencies in TADF OLEDs, as excitons form in a 25:75 singlet:triplet ratio upon electrical excitation. Typical rISC rates are on the order of 10^5 to 10^6 s^{-1} (compared to 10^2 to 10^4 s^{-1} for phosphorescence) and hence fluorescence from excitons that have undergone the rISC process has a lifetime in the microseconds domain [10].

Minimizing ΔE_{ST} can be achieved in TADF emitters with charge transfer (CT) excited states by imposing a spatial separation between the highest occupied and lowest unoccupied molecular orbitals (HOMO and LUMO, respectively). This can be realized by using electron donating (D) and accepting (A) units which are coupled via rigid and orthogonal spiroconjugation [11–15] or simply by ensuring a large dihedral angle between the D and A subunits through molecular design to increase steric hindrance [16–23]. The latter approach has received the most attention in recent years due to the greater design freedom in the choice and linkage patterns of the D and A moieties to form D-A or D-A-D structures. Using relatively weak D and A components, blue and green-emitting materials have been successfully developed, whereas stronger D and A units lead to the development of orange and red-emitting materials. If the energy of the localized excited (LE) triplet excited states of the D or A is significantly below that of the CT triplet states (and if non-radiative decay is negligible), emission from these LE states can sometimes be observed as room temperature phosphorescence (RTP), in competition with or instead of TADF [24–30]. These RTP emitters typically show a relatively low triplet emission quantum yield, rendering them inefficient for OLEDs. Nonetheless, their long-lived and often red-shifted emission can still be useful for other applications such as bio-imaging [27,31,32], sensing applications [33,34] or glow-in-the-dark [35] and security inks [36].

As the spin conversion processes are forbidden between orbitals of the same nature, ISC and rISC are very slow in traditional organic emitters [37]. Phosphorescent emitters make use of the large spin-orbit coupling (SOC) induced by the heavy-metal atoms to improve the ISC and phosphorescence emission rates. TADF emitters instead rely on the presence of isoenergetic and vibronically coupled triplet states to allow state mixing and to create triplet states with mixed CT and LE character [38,39]. These coupled states with small ΔE_{ST} allow for greatly enhanced (r)ISC rates. The mixing of the triplet states in D-A-D materials following the spin-vibronic mechanism for TADF is expected to occur via a vibrational rocking of the D with respect to the A unit [39–41].

A near infinite number of D-A-D materials can be prepared, with their color and TADF performance largely controlled by the choice of D and A. Inspired by the field of organic photovoltaics, where it is widely used in push-pull type conjugated polymers [42,43], benzo[1,2-*b*:4,5-*b*']dithiophene (BDT) was chosen here as a promising novel donor unit for TADF emitters. However, coupling the BDT unit via the conventional α-positions of the thiophene subunits would lead to largely planar D-A combinations – unsuitable for TADF. Therefore, in this work, 2,6-bis(triisopropylsilyl)benzo[1,2-*b*:4,5-*b*']dithiophene (BDT-TIPS) was used to construct D-A-D compounds with two different acceptors, 9,9-dimethyl-9*H*-thioxanthene-10,10-dioxide (TXO2) [19,23,44–46] and dibenzo[*a*,*c*]phenazine-11,12-dicarbonitrile (CNQxP) [47]. For comparison, the 9,9-dimethyl-9,10-dihydroacridine (DMAC) analogues were also synthesized and investigated.

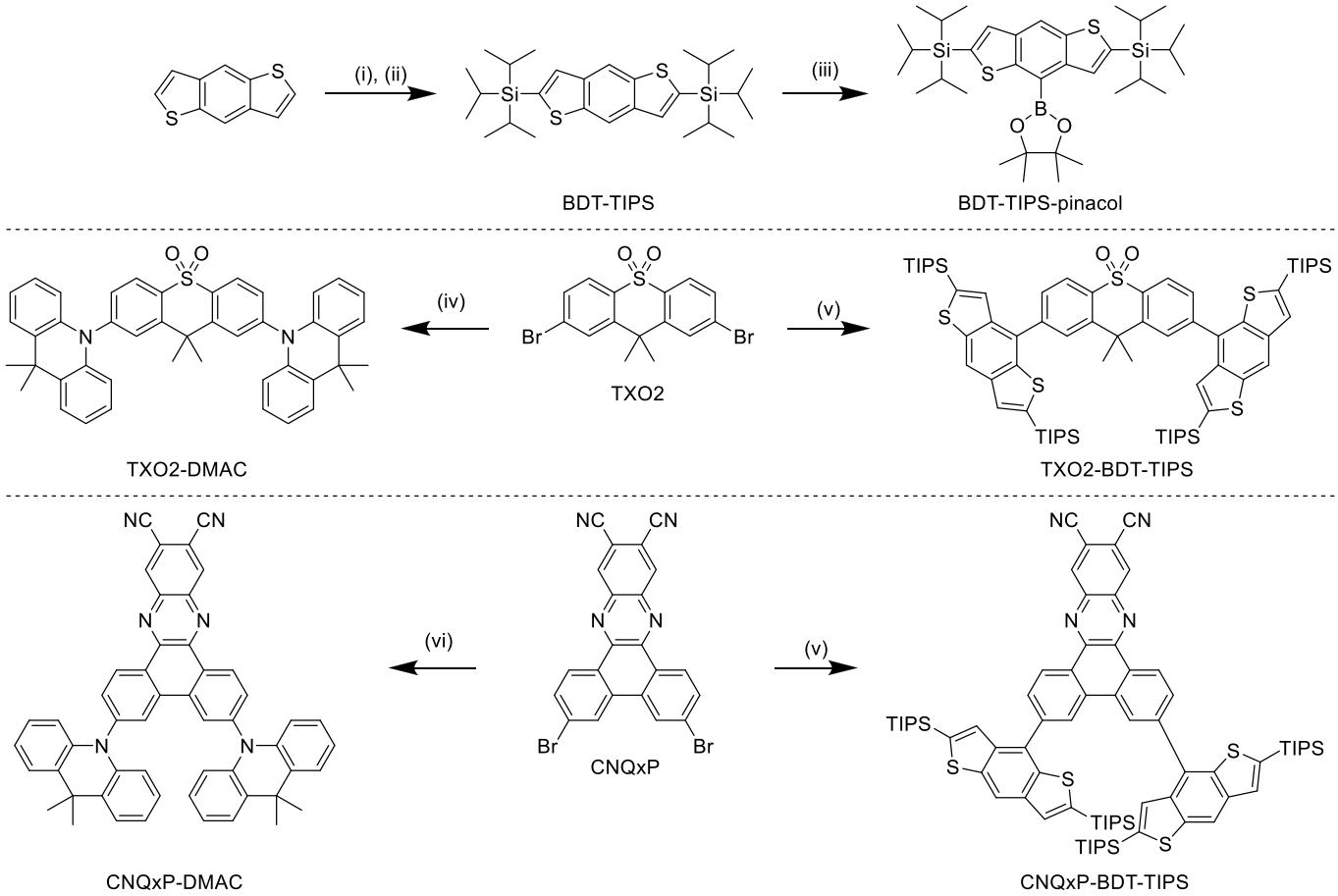

Scheme 1. Synthesis pathways for all studied compounds: (i) *n*-BuLi, THF, 0 °C, 1 h; (ii) TIPSCl, THF, reflux, 16 h; (iii) Bis(pinacolato)diboron, $[Ir(OMe)(COD)]_2$, 4,4′-di-*tert*-butyl-2,2′-bipyridine, cyclohexane, reflux, 24 h; (iv) 9,9-dimethyl-10*H*-acridine, $Pd_2(dba)_3$, $HPtBu_3BF_4$, NaO*t*Bu, toluene, reflux, 21 h; (v) BDT-TIPS-pinacol, $Pd(PPh_3)_4$, K_2CO_3, toluene/H_2O (4/1), 80 °C, 24 h; (vi) 9,9-dimethyl-10*H*-acridine, $Pd(OAc)_2$, $HPtBu_3BF_4$, NaO*t*Bu, toluene, reflux, 24 h.

2. Results and discussion

2.1. Material synthesis

The novel BDT-TIPS donor building block was synthesized as a boronic ester according to literature, as shown in Scheme 1 [48]. Triisopropylsilyl (TIPS) protection is necessary to prevent boroester formation on the thienyl 2- and 3-positions. Coupling to different acceptors was achieved using Suzuki-Miyaura cross-coupling, while Buchwald-Hartwig cross-coupling was used for the DMAC compounds. Full details of all synthetic procedures are included in the supporting information (SI).

2.2. Theoretical calculations

Geometry optimizations were performed on the isolated BDT-TIPS donor (Fig. S8) and the 4 different D-A-D emitters (Fig. 1) using DFT (M06/6-311G(d)). The excited state properties were calculated by TDDFT using LC-BLYP with a modified range-separating parameter ($\omega = 0.17\ a_0^{-1}$) as the exchange correlation (XC) functional [48,49]. TDDFT calculations were performed under the Tamm-Dancoff approximation and using the polarizable continuum model (PCM) in cyclohexane to simulate a non-polar environment in the Gaussian16 package [50]. The CT character of the involved states was investigated by looking at the differences of ground and excited state electron densities (Figs. S9 and S10). These were characterized by the distance over which charge is transferred, calculated according to the work of Le Bahers et al. [51], and the related change in dipole moment. For the geometry optimizations, the TIPS groups were explicitly included to accurately judge their influence on the electronic and structural properties. Although TXO2-DMAC has already been investigated before [23,44–46,52], it was included in the calculations to allow straightforward comparison between the DMAC and BDT-TIPS donor systems. The CNQxP acceptor is also known from literature and was previously used to construct D-A systems with phenyl-spaced DMAC and diphenylamine (DPA) units [47]. However, to the best of our knowledge, direct coupling between CNQxP and DMAC has not been reported before. A similar dibenzo[*f*,*h*]quinoxaline-2,3-dicarbonitrile entity was used to construct D-A-D systems containing DMAC (amongst other donors), but this acceptor has a lower electron affinity, providing slightly blue-shifted emission [53]. In these two examples, TADF was observed experimentally.

Large dihedral angles of around 90° were observed for the two DMAC-containing compounds (Table 1), leading to well-separated HOMO and LUMO distributions (Fig. 1). The two compounds with BDT-TIPS donor groups show considerably smaller dihedral angles of around 50°. This is not unexpected, since the central six-membered ring is flanked by two smaller five-membered rings, as opposed to the six-membered rings in DMAC, affording less steric control over the D-A dihedral angle [22]. The consequences of these smaller dihedral angles are also apparent looking at the HOMO and LUMO distributions (Fig. 1), with the BDT-TIPS compounds showing increased overlap between the HOMO and LUMO, in particular for TXO2, with the proximity of the two donor moieties in CNQxP-BDT-TIPS possibly leading to additional steric interactions. The smaller calculated dihedral angles for the BDT-TIPS compounds are consistent with larger oscillator strengths for the molecular $S_0 \rightarrow S_1$ transitions (having a largely dominant HOMO to LUMO character), along with their larger singlet-triplet energy gaps (Table 1).

TDDFT calculations were then performed to investigate excited singlet and triplet energies and their respective energy differences (Table 1). The TXO2-based compounds have S_1 excitation energies that are higher than those based on CNQxP, indicative of the lower acceptor strength of the TXO2 core. Similarly, the singlet energies of the compounds containing the BDT-TIPS donor are higher than for their DMAC counterparts, demonstrating the lower donor strength of the BDT-TIPS group. While all D-A-D compounds show small energy gaps between the first and second triplet energies ($\Delta E_{T_2-T_1}$), only the DMAC-containing compounds show a small calculated ΔE_{ST}. It is therefore anticipated that the BDT-TIPS donor will require highly sophisticated molecular design strategies to afford TADF behavior, to overcome its intrinsically small D-A angles and the associated large orbital overlap. To account for vibration-induced symmetry-breaking effects, additional TDDFT calculations were performed with modified dihedral angles (±10°), revealing the weak intensity of the low-energy transitions of the DMAC-based compounds, while the excitation energies and other excited state properties are only impacted in a negligible way (Fig. S1).

The CT nature of the first and second excited singlet and triplet states was also investigated (Table 2). TXO2-DMAC shows CT character in its first excited singlet and triplet states, as shown in Fig. S9. This property is associated with CT distance (d_{CT}) values of around 1.49 Å and relatively large change in dipole moment ($\Delta\mu$) upon excitation. This strong CT nature, combined with the small ΔE_{ST}, contributes significantly to the high EQEs (>20%) obtained with this TADF emitter [23,44,45,54].

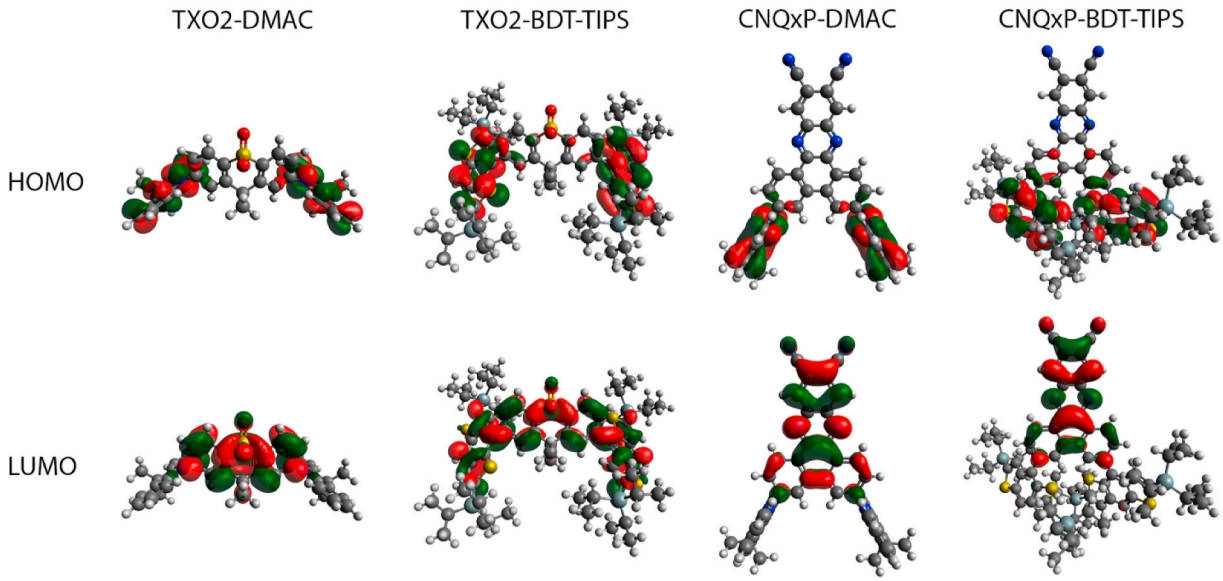

Fig. 1. HOMO and LUMO topologies obtained using LC-BLYP(ω = 0.17) for the optimized geometries of the different emitters investigated in this work. Isocontour values of 0.02 a. u. were used for all orbitals.

Table 1
TDDFT results for the first vertical singlet excitation energies and corresponding oscillator strengths, the first and second vertical triplet excitation energies and dihedral angles (obtained from DFT geometry optimization).

Compound	S_1 (eV)	f_{S_1}	S_2 (eV)	f_{S_2}	T_1 (eV)	T_2 (eV)	$\Delta E_{T_2-T_1}$ (eV)	$\Delta E_{S_1-T_1}$ (eV)	D-A angle (°)[a]
TXO2-DMAC	3.26	0.00 (0.03)[b]	3.26	0.00 (0.01)[b]	3.24	3.25	0.01	0.02	90
TXO2-BDT-TIPS	3.57	0.60	3.62	0.12	2.64	2.65	0.01	0.93	54
CNQxP-DMAC	2.49	0.00 (0.01)[b]	2.50	0.00 (0.05)[b]	2.47	2.50	0.03	0.02	90
CNQxP-BDT-TIPS	2.92	0.64	2.99	0.08	2.47	2.49	0.02	0.45	48
BDT-TIPS	3.87	0.31	4.32	0.35	2.80	3.58	0.78	1.17	/

[a] Taken as the average of 4 possible torsion angles.
[b] Oscillator strengths when the D-A dihedral angle is modified by ±10°.

Table 2
Nature of the various transitions, charge transfer distance (d_{CT}) and change in dipole moment ($\Delta\mu$, excited – ground state dipole) accompanying the S_0- > S_x and S_0- > T_x transitions in cyclohexane.

Compound	S1			S2			T1			T2		
	Nature	d_{CT} (Å)	$\Delta\mu$ (D)	Nature	d_{CT} (Å)	$\Delta\mu$ (D)	Nature	d_{CT} (Å)	$\Delta\mu$ (D)	Nature	d_{CT} (Å)	$\Delta\mu$ (D)
TXO2-DMAC	H → L	1.49	8.18	H-1 → L	1.49	8.19	H → L	1.48	8.14	H-1 → L	1.49	8.15
TXO2-BDT-TIPS	H → L	0.96	2.70	H-1 → L	0.92	2.47	H → L	0.40	0.79	H-1 → L	0.41	0.80
CNQxP-DMAC	H → L	4.18	24.64	H-1 → L	4.08	24.18	H → L	4.04	21.54	H-1 → L	4.17	24.76
CNQxP-BDT-TIPS	H → L	3.96	17.78	H-1 → L	3.79	16.66	H → L	2.98	8.19	H-1 → L	2.46	5.77

TXO2-BDT-TIPS, on the other hand, shows more localized excitations for both the singlet and triplet excited states, as shown in Fig. S9 and as indicated by the much smaller d_{CT} and $\Delta\mu$ values. This localized excitonic nature arises from the shared LUMO distribution on the BDT-TIPS and acceptor units, whereas for TXO2-DMAC the LUMO resides entirely on the TXO2 part. Despite having two triplet states in close proximity, the large ΔE_{ST} restricts the possibility for TADF to occur in TXO2-BDT-TIPS. Like TXO2-DMAC, CNQxP-DMAC also shows good HOMO-LUMO separation and a small ΔE_{ST}. The first singlet and triplet excited states also show strong CT character, with large values for d_{CT} and $\Delta\mu$. For CNQxP-BDT-TIPS, the situation is less straightforward. Whereas the two first singlet excited states show strong CT character, the first and second triplet excited states have mixed charge-transfer (CT) and localized excited (LE) state character (due to contributions of multiple one-particle transitions) as they show intermediate d_{CT} and $\Delta\mu$ values (Fig. S10).

2.3. Photophysics

The steady-state absorption and emission spectra of the BDT-TIPS containing D-A-D materials in 1 wt% doped zeonex films show large differences in absorption and emission energy, due to the different electron-withdrawing strengths of the TXO2 and CNQxP acceptor units (Fig. 2). TXO2-DMAC [23,44–46,52,54] has been studied in this host before, and data are presented here too to enable direct comparison to TXO2-BDT-TIPS. Both materials containing CNQxP have structured low energy absorption bands, corresponding to ππ* transitions of the CNQxP unit with some D-A CT character, and are slightly shifted with respect to each other due to the different electron-donating properties of the DMAC and BDT groups. The BDT-TIPS and DMAC donor units also have a large influence on the D-A-D emission wavelengths, with the DMAC-based materials showing emission maxima red-shifted by 19 nm (0.12 eV) for TXO2 and 68 nm (0.22 eV) for CNQxP compared to the BDT-TIPS analogues. This is in line with the stronger donor character for the DMAC group, leading to a larger CT character of the emission and lower energy emission. These findings are in line with the results from the TDDFT calculations, as also evidenced by the simulated absorption spectra (Fig. S1). The emission spectrum for TXO2-BDT-TIPS is quite narrow in comparison to that of TXO2-DMAC, suggesting a more localized nature of the emission. On the other hand, the emission spectra for both CNQxP-based compounds are broad, suggesting predominant CT character. The CNQxP-BDT-TIPS emission is unique in that it shows some structure and its onset is very close to the absorption edge, which could be due to dual emission of a higher energy ^{1}LE and lower ^{1}CT state. Indeed, separate emission bands corresponding to the shoulder and peak of the steady-state emission are observed in time-resolved measurements (Fig. S3), supporting this assignment.

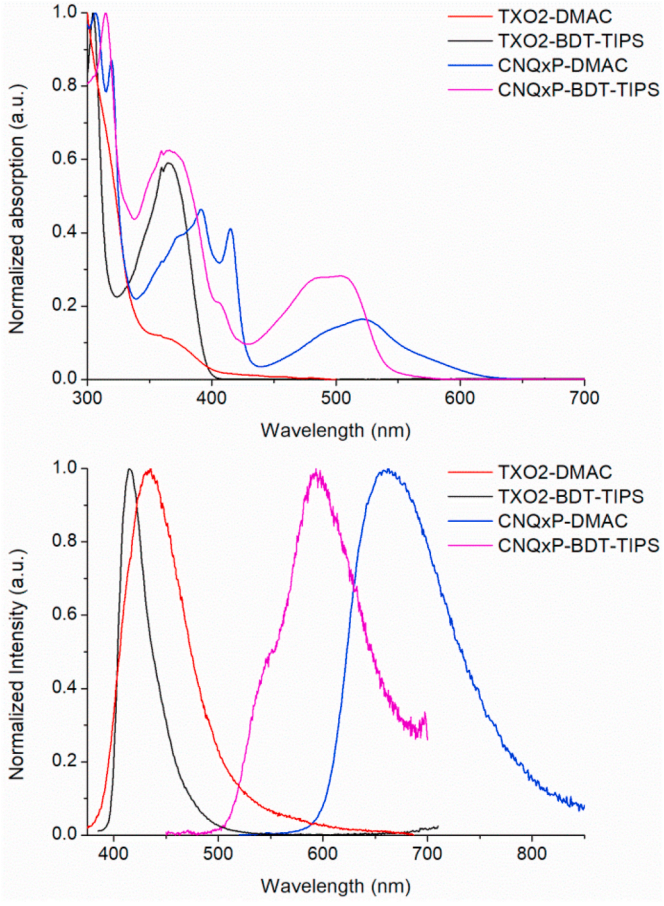

Fig. 2. Steady-state absorption (top) and emission (bottom) spectra at room temperature in zeonex film.

Time-dependent emission spectra and decays were then obtained using a pulsed laser and iCCD camera to investigate the dynamic photophysics in these systems. From the contour plots of the normalized spectra and the total emission decays in zeonex (Fig. 3a,c; spectra in Fig. S2), it is apparent that TXO2-BDT-TIPS has no delayed emission in the microseconds regime (the spectra in Fig. 3a in this time region are consistent with normalized CCD baseline signal). High-energy LE emission consistent with the steady-state photoluminescence (PL) is observed at first, which relaxes over the first 50 ns to a red-shifted CT state before emission falls below the sensitivity limit of the instrument. A longer living and further red-shifted emission spanning into the milliseconds domain is then observed. Comparing the millisecond emission spectra at room temperature and at 80 K (Fig. 4 bottom), it is apparent that the room temperature and 80 K emission come from the same state in TXO2-BDT-TIPS and are therefore both attributed to phosphorescence. From the onset of the prompt fluorescence (PF) at room temperature and the phosphorescence at 80 K, the singlet and triplet energies and the corresponding singlet-triplet energy gap were calculated (Table 3). With an experimental ΔE_{ST} of 0.78 eV (vs. 0.93 eV calculated), TADF is excluded as a possible delayed fluorescence (DF) emission mechanism in TXO2-BDT-TIPS. The occurrence of RTP is attributed to the presence of the BDT-TIPS donor, as this emission mechanism was not observed for TXO2-DMAC (Fig. 3b).

For CNQxP-BDT-TIPS, a combination of LE and CT emission seems to

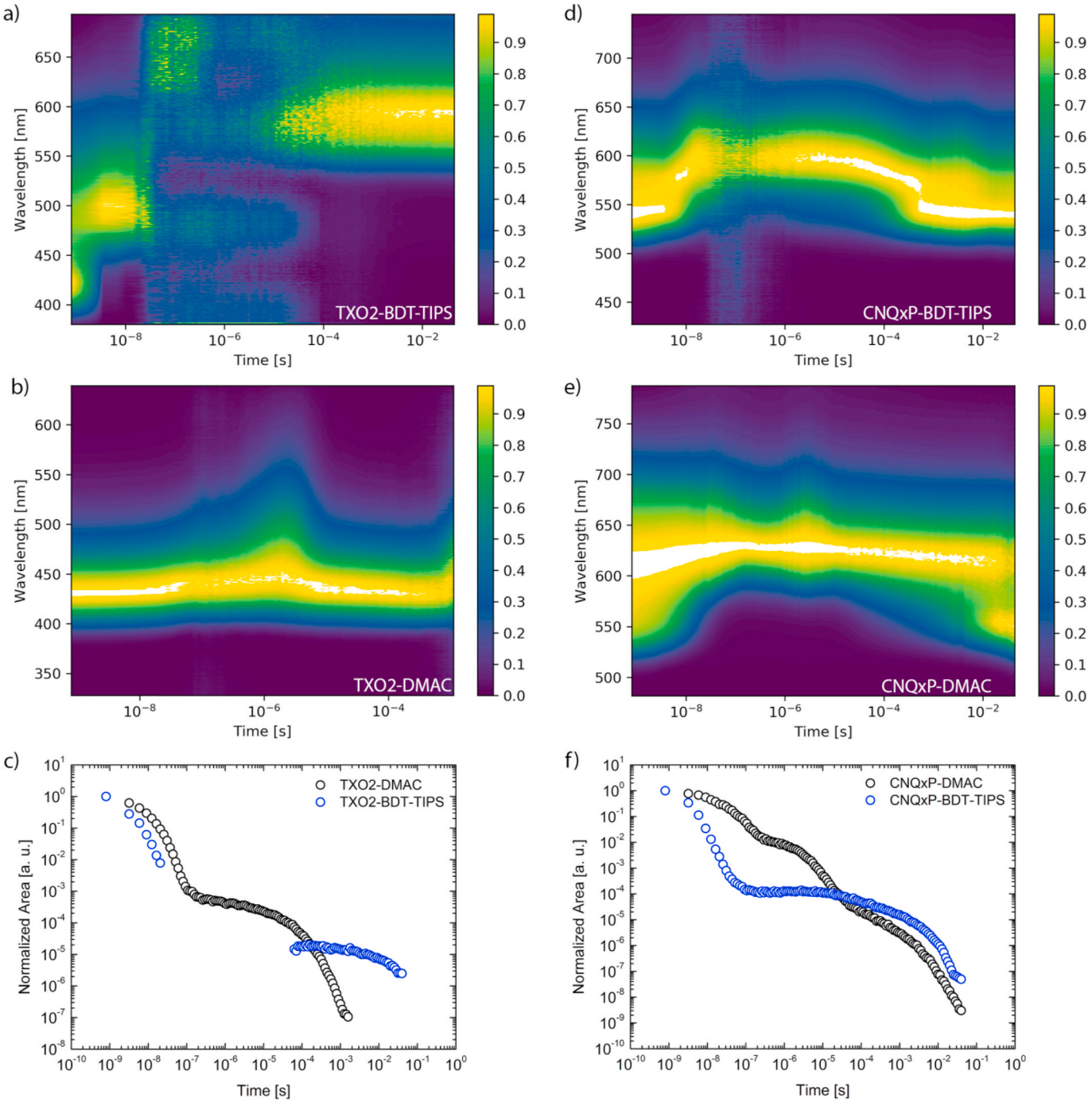

Fig. 3. Contour plots for the normalized room temperature time-resolved emission spectra of TXO2-BDT-TIPS (a), TXO2-DMAC (b), CNQxP-BDT-TIPS (d) and CNQxP-DMAC (e) in zeonex, along with the emission intensity decays (c and f).

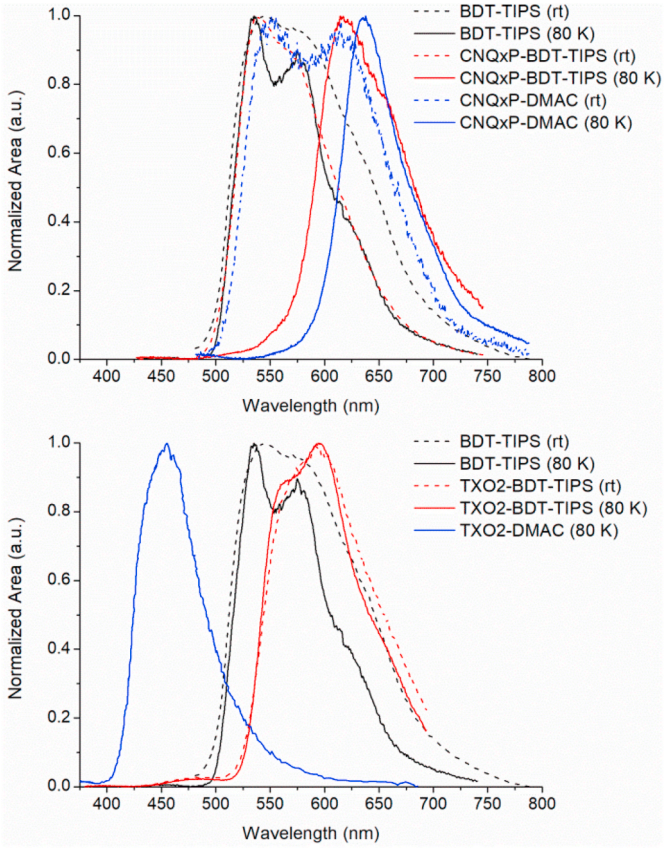

Fig. 4. Emission spectra obtained at a 44.7 ms delay for BDT-TIPS, CNQxP-BDT-TIPS and CNQxP-DMAC (top), and for BDT-TIPS, TXO2-BDT-TIPS and TXO2-DMAC (bottom) at 80 K and at room temperature.

be present at early decay times (Fig. S3), which implies a reduced electron transfer rate to form the CT state compared to the other materials. Like in TXO2-BDT-TIPS, this is probably due to the BDT group having moderate dihedral angles with respect to the acceptor unit and having a rather weak electron-donating strength (as judged by comparison of the PL color to the DMAC compounds). As the "LE" emission dies out, the CT emission remains throughout the remainder of the decay, although at very long times (>1 ms) the "LE" emission seemingly reappears. The same short-wavelength emission is present at early decay times at 80 K, but does not reappear near the end of the decay (Fig. S3). Furthermore, the microsecond emission present at room temperature is absent at 80 K. At long times in the decay at 80 K, a red-shifted emission is seen, which is attributed to the true phosphorescence of the system (Fig. S3). The absence of the microsecond emission at 80 K demonstrates temperature dependency as expected for TADF emission. The singlet (2.35 eV) and triplet (2.17 eV) emission energies from the experimental data lead to a singlet-triplet gap of 0.18 eV, which is large but not insurmountable at room temperature (Table 3) [52]. The red-shifted microsecond emission in zeonex at room temperature has an onset of around 2.30 eV, indicating that TADF is a potential emission pathway. The blue-shifted millisecond emission in CNQxP-BDT-TIPS is instead suggested to arise from triplet-triplet annihilation (TTA) and subsequent emission from singlet LE states. The same LE states are also formed directly following photoexcitation, which is why they share the same spectra at very early and very late decay times. The signal arising from TTA is long lived but weak, and so it is only observable once the TADF emission has decayed substantially, and is completely suppressed at low temperatures which restrict triplet migration through the film. This assignment is also verified by the TDDFT calculations. Due to the apparent symmetry in the system, S_1 and S_2 are of HOMO and HOMO-1 to LUMO character, respectively, and consist of D → A CT transitions (Fig. S10). The third excited singlet state (S_3) represents the first singlet excited state with a localized character and has an energy that is only 0.12 eV (17 nm) higher than that of S_1 (Table S1). Furthermore, S_3 is localized on the CNQxP acceptor unit (Fig. S10). With an S_1 energy of 3.00 eV for the CNQxP unit (Table S2), the position of the S_3 state of CNQxP-BDT-TIPS is confirmed, suggesting S_3 to be the LE state that we observed in the experimental time-resolved decays at early and long times. Similarly, the first two excited triplet states (T_1, T_2) are D → A CT transitions whereas T_3 is localized on the acceptor and is 0.15 eV higher in energy than T_1 (Table S1, Fig. S10). According to the spin-vibronic mechanism for TADF, these states have the potential to mix and decrease the effective ΔE_{ST}. While the theoretical $\Delta E_{S1\text{-}T1}$ is rather large (0.45 eV), the experimental energy gap (0.18 eV) is not and considering the precision of the TDDFT calculations and the fact that excited state relaxation is not taken into account, this mechanism is viable.

CNQxP-DMAC has consistent emission throughout the decay with an onset of about 2.15 eV (577 nm) in the microseconds regime. A short-wavelength contribution is present at very early decay times and reappears in the very long millisecond emission, similar to that of CNQxP-BDT-TIPS (Fig. 3e). At 80 K, the emission is slightly red-shifted and the short-wavelength contribution at the start of the decay is less intense and does not reappear at longer times (Fig. S4). Even at 80 K, delayed emission is present at all times throughout the decay. As the onset of the spectra also remains the same, this is indicative of TADF emission with a very small ΔE_{ST}, as supported by the experimental determination of the singlet and triplet energies (Table 3). This is unusual as the TADF seemingly persists at 80 K, whereas the low wavelength emission is suppressed. We suggest that the very delayed high-energy emission is also generated by TTA and subsequent emission from LE states that are initially formed by photoexcitation as the position and localization of the S_3 state of **CNQxP-DMAC** is similar to that of **CNQxP-BDT-TIPS**. Additionally, the full decay of **CNQxP-DMAC** (Fig. 3f) shows two regions of increased intensity at around 10^{-6} and 10^{-3} s, while Fig. 3e shows delayed emission at a constant wavelength. Whereas the first

Table 3
Experimental photophysical properties and kinetics for TXO2-DMAC, TXO2-BDT-TIPS, CNQxP-DMAC and CNQxP-BDT-TIPS in zeonex.

Compound	E_S (eV)[a]	E_T (eV)[b]	ΔE_{ST} (eV)[c]	τ_{Fp} (ns)[d]	τ_{Fd} (μs)[e]	k_{ISC}[f]	k_{rISC}[f]
TXO2-DMAC	3.20	3.02	0.18	12.71	67.89	5.44×10^7	4.27×10^4
TXO2-BDT-TIPS	3.14	2.36	0.78	4.51	2.69×10^4	/[g]	/[g]
CNQxP-DMAC	2.07	2.09	−0.02	52.66	$4.67/1.80 \times 10^3$	1.04×10^7	5.17×10^5
CNQxP-BDT-TIPS	2.35	2.17	0.18	2.12	1.86×10^3	/[g]	/[g]
BDT-TIPS	3.24	2.48	0.76	0.78	4.40×10^4	/[g]	/[g]

[a] Taken from the onset of the prompt fluorescence (PF) emission.
[b] Taken from the onset of the phosphorescence emission at ms timescales at 80 K.
[c] Calculated as $E_s - E_T$.
[d] Lifetime of prompt fluorescence (F_p).
[e] Lifetime of delayed fluorescence (F_d).
[f] k_{ISC} and k_{rISC} rates were determined using kinetic fitting of the PF and DF emission according to the literature [46].
[g] Due to the lack of microsecond emission and/or unambiguous identification of a pure TADF mechanism, kinetic fitting was not performed.

region can be attributed to TADF, the second region appears at earlier times with respect to the onset of TTA ($>10^{-3}$ s). This is also unusual and may indicate the presence of two singlet excited states close in energy, as was also found using TDDFT calculations, showing TADF with largely varying k_{rISC} values.

To better understand the positioning of LE states in these materials, the BDT-TIPS donor itself was also embedded in a zeonex matrix and its time-dependent emission was recorded at room temperature and at 80 K (Fig. 4 and S5). As suggested by the calculations, the singlet and triplet emission are well separated with onsets at 3.24 and 2.48 eV, respectively (Table 3). It is remarkable how the BDT-TIPS group itself shows emission at several tens of milliseconds, even at room temperature. Comparing the spectra at room temperature and at 80 K shows that both the prompt and millisecond emission have the same onset at each temperature, and are thus coming from the same states in both cases. This is attributed to the presence of the sulphur atoms in the BDT core, which enhance SOC when compared to commonly used atoms such as carbon and nitrogen. Having two of these sulphur atoms could boost the SOC enough to enhance ISC from the S_1 to the T_1 state and subsequently enable the strong RTP observed in the donor fragment.

For TXO2-BDT-TIPS, it is possible that the observed RTP is coming from localized emission corresponding to the BDT-TIPS unit (Fig. 4). When looking at the pure BDT-TIPS and TXO2-BDT-TIPS spectra at room temperature and at 80 K, the similarities in the peak shape and onset indicates that emission is coming from similar states in both materials. The difference in onset could be due to the acceptor properties of TXO2, slightly lowering the BDT triplet energy level in the D-A-D compound, or from the vibrational mode of the highest energy vibronic peak in the BDT-TIPS phosphorescence spectrum being suppressed in the D-A-D material. Furthermore, the ground–excited state electron density differences predict the T_1 and T_2 states to be localized on the BDT-TIPS group (Fig. S9). CNQxP-BDT-TIPS behaves differently, as microsecond emission (attributed to TADF) is also observed. The large difference in the onset of the emission at several milliseconds at room temperature and at 80 K allows us to exclude RTP for this compound. One of the reasons is that the CT triplet of the D-A-D compound has a lower energy than the localized BDT-TIPS triplet state and coupling to the ground state from the CT triplet state is inefficient. Alternatively, rISC could be competing with the radiative relaxation from the T_1 state due to the smaller ΔE_{ST} with respect to TXO2-BDT-TIPS and the improved SOC. The ground–excited state electron density differences (Fig. S10) show significant CT character for the lowest excited triplet state, supporting this hypothesis.

The short-wavelength emission at a few nanoseconds in the decays of CNQxP-BDT-TIPS (Fig. 5) and CNQxP-DMAC (Fig. S4) is attributed to the presence of a locally excited singlet state (^{1}LE) above the TADF-active CT singlet (*vide supra*). The sterically hindered conformation in which the donor units reside likely slows down electron transfer and hence the internal conversion of the photoexcited ^{1}LE state to the lower ^{1}CT state. This is especially true at 80 K, where nuclear motion is further restricted and the prompt emission exhibits dual character over a longer time span. To explain the reoccurring short-wavelength ^{1}LE emission at long lifetimes, we identify TTA as the most likely mechanism. Having a much longer lifetime than TADF, TTA typically occurs in the milliseconds domain and requires two molecules to be in close proximity. In TTA, two triplet excitons are up-converted into one singlet exciton of higher energy, and even though the emitter is doped at only 1 wt% in zeonex, it is plausible that weak TTA is observed at very long times (once brighter and faster-decaying emission from TADF-active states is depleted). Because the energy of two triplet excitons is larger than the energy of the ^{1}LE state, this state can be populated. Loss of the red emission edge at several tens of milliseconds for CNQxP-BDT-TIPS suggests that as TADF emission dies out, the emission band becomes dominated by pure ^{1}LE emission with significant vibronic character. CNQxP-DMAC does not lose its red emission edge and is therefore a combination of both ^{1}LE and ^{1}CT emission even at very long lifetimes -

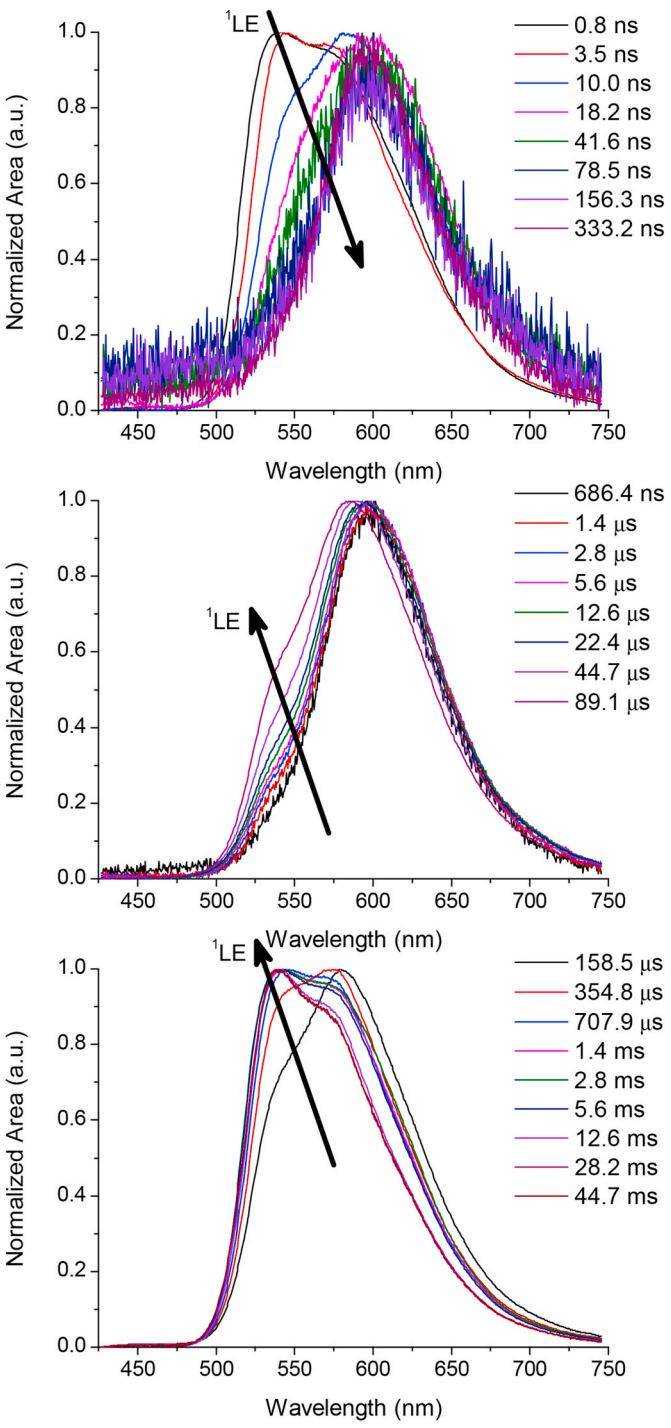

Fig. 5. Time-resolved emission extracted from the room temperature decay of CNQxP-BDT-TIPS showing the slow transfer from ^{1}LE to ^{1}CT emission at short lifetimes and the reappearance of pure ^{1}LE emission at very long lifetimes.

resulting from TTA and very long-lived TADF, respectively. In CNQxP-BDT-TIPS, which also has a larger ΔE_{ST}, TTA seems to be more intense as it starts to appear at earlier decay times and becomes more prominent in the longer milliseconds regime. The absence of LE emission in the milliseconds domain for both compounds at 80 K is also consistent with either a TADF or TTA mechanism, as these processes are typically both inhibited at lower temperatures. However, as stated before, CNQxP-DMAC seemingly shows TADF emission even at 80 K.

2.4. Laser power experiments

To verify a TADF mechanism in the microseconds domain in both CNQxP compounds, the dependence of emission intensity on excitation laser power was measured by attenuation of the excitation beam with reflective neutral density filters. Both compounds were probed with a delay time after the laser pulse of 4 μs and an integration time of 12 μs Even at very low powers (0.2 μJ vs. 78.0 μJ at the start of the measurement), the slope of the log-log plot remains unity, suggesting TADF-like behavior. In the case of TTA, we would expect this slope to increase at low excitation power (second order with the exciton density). Similar measurements at longer delay times reveal that the slopes become slightly larger (Figs. S6b and d), which could indicate the presence of a TTA emission contribution at very long times. However as we observe a combination with TADF at these delay times, we still do not observe a gradient of 2 that is otherwise indicative of 'pure' TTA emission (Figs. S7b and d).

3. Conclusions

In this work, we have introduced a triisopropyl-substituted benzo[1,2-*b*:4,5-*b*']dithiophene (BDT-TIPS) donor unit that is directly coupled via the central phenyl moiety, giving rise to two new donor-acceptor-donor emitters. In contrast with analogous 9,9-dimethyl-9,10-dihydroacridine (DMAC) containing compounds, TXO2-BDT-TIPS was found to show room temperature phosphorescence as a result of a low-lying localized triplet state on the BDT-TIPS group itself. The BDT-TIPS precursor was investigated and was found to also exhibit phosphorescence at room temperature, presumably due to the sulphur atoms that afford increased spin-orbit coupling and thereby enhance the radiative $T_1 \rightarrow S_0$ relaxation. The CNQxP-DMAC chromophore prepared in this work was found to show TADF, with a very small ΔE_{ST} value giving rise to delayed emission even at 80 K. Its BDT-TIPS counterpart also showed delayed emission attributed to TADF. Despite a larger ΔE_{ST} (0.18 eV) than its DMAC counterpart, the BDT-TIPS unit promotes (r)ISC by increased spin-orbit coupling in the CNQxP compound, leading to long-lived orange TADF. At longer times, triplet-triplet annihilation (TTA) repopulating the ^{1}LE state gives rise to resurgent short-wavelength LE emission for both CNQxP materials.

Although RTP and very long lived TADF/TTA emission are not desirable for OLED applications, the long-lived and red-shifted emission for TXO2-BDT-TIPS and CNQxP-BDT-TIPS may find future use in other applications such as imaging or sensing [55–57]. Furthermore, the BDT-TIPS donor investigated here represents a valuable addition to the library of available donor compounds for TADF, particularly suitable to generate deep-blue emission.

Supporting information

Detailed information on the synthesis procedures, ^{1}H and ^{13}C NMR spectra, additional TDDFT calculations, time-resolved photoluminescence spectra, laser power measurements, HOMO and LUMO topologies for BDT-TIPS, ground/excited state electron density differences, and coordinates of the optimized geometries can be found in the supporting information.

CRediT authorship contribution statement

Tom Cardeynaels: Writing – original draft, Synthesis and structural characterization of all compounds, quantum-chemical calculations, spectroscopic measurements and preparation of the manuscript. **Simon Paredis:** Writing – original draft, Spectroscopic measurements, discussion and revision of the manuscript. **Andrew Danos:** Supervision, Writing – original draft, of time-resolved spectroscopy, discussion and revision of the manuscript. **Dirk Vanderzande:** Writing – original draft, and. **Andrew P. Monkman:** Supervision, Writing – original draft, of time-resolved spectroscopy at Durham University facilities, discussion of the results and revision of the manuscript. **Benoît Champagne:** Writing - review and editing, Supervison, Funding acquisition, of the quantum-chemical calculations, discussion of the results and revision of the manuscript. **Wouter Maes:** Writing - review and editing, Supervison, Funding acquisition, discussion of the results and revision of the manuscript.

Declaration of competing interest

The authors declare that they have no known competing financial interests or personal relationships that could have appeared to influence the work reported in this paper.

Acknowledgements

This work is supported by the University of Namur and Hasselt University [PhD BILA scholarship T. Cardeynaels]. The authors also thank the Research Foundation – Flanders (FWO Vlaanderen) for financial support [project G.0877.18 N, Hercules project GOH3816-NAUHL, and SB PhD scholarship S. Paredis]. The calculations were performed on the computers of the « Consortium des équipements de Calcul Intensif *(CÉCI)* » (http://www.ceci-hpc.be), including those of the « UNamur Technological Platform of High-Performance Computing (PTCI) » (http://www.ptci.unamur.be), for which we gratefully acknowledge the financial support from the FNRS-FRFC, the Walloon Region, and the University of Namur [Conventions No. 2.5020.11, GEQ U.G006.15, U.G018.19, 1610468, and RW/GEQ2016]. A. Danos and A. P. Monkman are supported by EU Horizon 2020 Grant Agreement No. 732013 (HyperOLED). We thank Alastair Harrison for assistance in collecting spectroscopic data for TXO2-DMAC.

Appendix A. Supplementary data

Supplementary data to this article can be found online at https://doi.org/10.1016/j.dyepig.2020.109022.

References

[1] Jou J-H, Kumar S, Agrawal A, Li T-H, Sahoo S. Approaches for fabricating high efficiency organic light emitting diodes. J Mater Chem C 2015;3(13):2974–3002.
[2] Hyocheol J, Hwangyu S, Jaehyun L, Beomjin K, Young-Il P, Kyoung Soo Y, et al. Recent progress in the use of fluorescent and phosphorescent organic compounds for organic light-emitting diode lighting. J Photon Energy 2015;5(1):1–23.
[3] Geffroy B, le Roy P, Prat C. Organic light-emitting diode (OLED) technology: materials, devices and display technologies. Polym Int 2006;55(6):572–82.
[4] Thejokalyani N, Dhoble SJ. Novel approaches for energy efficient solid state lighting by RGB organic light emitting diodes – a review. Renew Sustain Energy Rev 2014;32:448–67.
[5] Brütting W, Frischeisen J, Schmidt TD, Scholz BJ, Mayr C. Device efficiency of organic light-emitting diodes: progress by improved light outcoupling. Phys Status Solidi 2013;210(1):44–65.
[6] Bizzarri C, Hundemer F, Busch J, Bräse S. Triplet emitters versus TADF emitters in OLEDs: a comparative study. Polyhedron 2018;140:51–66.
[7] Seo H-J, Yoo K-M, Song M, Park JS, Jin S-H, Kim YI, et al. Deep-blue phosphorescent iridium complexes with picolinic acid N-oxide as the ancillary ligand for high efficiency organic light-emitting diodes. Org Electron 2010;11(4):564–72.
[8] Hofmann S, Thomschke M, Freitag P, Furno M, Lüssem B, Leo K. Top-emitting organic light-emitting diodes: influence of cavity design. Appl Phys Lett 2010;97(25):253308.
[9] Adachi C. Third-generation organic electroluminescence materials. Jpn J Appl Phys 2014;53(6):060101.
[10] Penfold TJ, Dias FB, Monkman AP. The theory of thermally activated delayed fluorescence for organic light emitting diodes. Chem Commun 2018;54(32):3926–35.
[11] Kawasumi K, Wu T, Zhu T, Chae HS, Van Voorhis T, Baldo MA, et al. Thermally activated delayed fluorescence materials based on homoconjugation effect of donor–acceptor triptycenes. J Am Chem Soc 2015;137(37):11908–11.
[12] Ohkuma H, Nakagawa T, Shizu K, Yasuda T, Adachi C. Thermally activated delayed fluorescence from a spiro-diazafluorene derivative. Chem Lett 2014;43(7):1017–9.

[13] Nasu K, Nakagawa T, Nomura H, Lin C-J, Cheng C-H, Tseng M-R, et al. A highly luminescent spiro-anthracenone-based organic light-emitting diode exhibiting thermally activated delayed fluorescence. Chem Commun 2013;49(88):10385–7.
[14] Nakagawa T, Ku S-Y, Wong K-T, Adachi C. Electroluminescence based on thermally activated delayed fluorescence generated by a spirobifluorene donor–acceptor structure. Chem Commun 2012;48(77):9580–2.
[15] Méhes G, Nomura H, Zhang Q, Nakagawa T, Adachi C. Enhanced electroluminescence efficiency in a spiro-acridine derivative through thermally activated delayed fluorescence. Angew Chem Int Ed 2012;51(45):11311–5.
[16] Lee J, Shizu K, Tanaka H, Nomura H, Yasuda T, Adachi C. Oxadiazole- and triazole-based highly-efficient thermally activated delayed fluorescence emitters for organic light-emitting diodes. J Mater Chem C 2013;1(30):4599–604.
[17] Taneda M, Shizu K, Tanaka H, Adachi C. High efficiency thermally activated delayed fluorescence based on 1,3,5-tris(4-(diphenylamino)phenyl)-2,4,6-tricyanobenzene. Chem Commun 2015;51(24):5028–31.
[18] Uoyama H, Goushi K, Shizu K, Nomura H, Adachi C. Highly efficient organic light-emitting diodes from delayed fluorescence. Nature 2012;492(7428):234–8.
[19] Dos Santos PL, Ward JS, Data P, Batsanov AS, Bryce MR, Dias FB, et al. Engineering the singlet–triplet energy splitting in a TADF molecule. J Mater Chem C 2016;4(17):3815–24.
[20] Dias FB, Bourdakos KN, Jankus V, Moss KC, Kamtekar KT, Bhalla V, et al. Triplet harvesting with 100% efficiency by way of thermally activated delayed fluorescence in charge transfer OLED emitters. Adv Mater 2013;25(27):3707–14.
[21] Pashazadeh R, Pander P, Lazauskas A, Dias FB, Grazulevicius JV. Multicolor luminescence switching and controllable thermally activated delayed fluorescence turn on/turn off in carbazole–quinoxaline–carbazole triads. J Phys Chem Lett 2018;9(5):1172–7.
[22] Kukhta NA, Higginbotham HF, Matulaitis T, Danos A, Bismillah AN, Haase N, et al. Revealing resonance effects and intramolecular dipole interactions in the positional isomers of benzonitrile-core thermally activated delayed fluorescence materials. J Mater Chem C 2019;7(30):9184–94.
[23] Stachelek P, Ward JS, dos Santos PL, Danos A, Colella M, Haase N, et al. Molecular design strategies for color tuning of blue TADF emitters. ACS Appl Mater Interfaces 2019;11(30):27125–33.
[24] Chen C, Huang R, Batsanov AS, Pander P, Hsu Y-T, Chi Z, et al. Intramolecular charge transfer controls switching between room temperature phosphorescence and thermally activated delayed fluorescence. Angew Chem Int Ed 2018;57(50):16407–11.
[25] Gong Y, Chen G, Peng Q, Yuan WZ, Xie Y, Li S, et al. Achieving persistent room temperature phosphorescence and remarkable mechanochromism from pure organic luminogens. Adv Mater 2015;27(40):6195–201.
[26] Hirata S, Totani K, Zhang J, Yamashita T, Kaji H, Marder SR, et al. Efficient persistent room temperature phosphorescence in organic amorphous materials under ambient conditions. Adv Funct Mater 2013;23(27):3386–97.
[27] Ni F, Zhu Z, Tong X, Xie M, Zhao Q, Zhong C, et al. Organic emitter integrating aggregation-induced delayed fluorescence and room-temperature phosphorescence characteristics, and its application in time-resolved luminescence imaging. Chem Sci 2018;9(28):6150–5.
[28] Pander P, Swist A, Motyka R, Soloducho J, Dias FB, Data P. Thermally activated delayed fluorescence with a narrow emission spectrum and organic room temperature phosphorescence by controlling spin–orbit coupling and phosphorescence lifetime of metal-free organic molecules. J Mater Chem C 2018;6(20):5434–43.
[29] Ward JS, Nobuyasu RS, Batsanov AS, Data P, Monkman AP, Dias FB, et al. The interplay of thermally activated delayed fluorescence (TADF) and room temperature organic phosphorescence in sterically-constrained donor–acceptor charge-transfer molecules. Chem Commun 2016;52(12):2612–5.
[30] Yu L, Wu Z, Zhong C, Xie G, Zhu Z, Ma D, et al. Pure organic emitter with simultaneous thermally activated delayed fluorescence and room-temperature phosphorescence: thermal-controlled triplet recycling channels. Advanced Optical Materials 2017;5(24):1700588.
[31] Fateminia SMA, Mao Z, Xu S, Yang Z, Chi Z, Liu B. Organic nanocrystals with bright red persistent room-temperature phosphorescence for biological applications. Angew Chem Int Ed 2017;56(40):12160–4.
[32] Zhang G, Palmer GM, Dewhirst MW, Fraser CL. A dual-emissive-materials design concept enables tumour hypoxia imaging. Nat Mater 2009;8(9):747–51.
[33] Lehner P, Staudinger C, Borisov SM, Klimant I. Ultra-sensitive optical oxygen sensors for characterization of nearly anoxic systems. Nat Commun 2014;5(1):4460.
[34] Lee D, Bolton O, Kim BC, Youk JH, Takayama S, Kim J. Room temperature phosphorescence of metal-free organic materials in amorphous polymer matrices. J Am Chem Soc 2013;135(16):6325–9.
[35] Jinnai K, Kabe R, Adachi C. Wide-range tuning and enhancement of organic long-persistent luminescence using emitter dopants. Adv Mater 2018;30(38):1800365.
[36] Li H, Ye S, Guo JQ, Kong J-T, Song J, Kang Z-H, et al. The design of room-temperature-phosphorescent carbon dots and their application as a security ink. J Mater Chem C 2019;7(34):10605–12.
[37] Baba M. Intersystem crossing in the 1npi* and 1pipi* states. J Phys Chem 2011;115(34):9514–9.
[38] de Sa Pereira D, Menelaou C, Danos A, Marian C, Monkman AP. Electroabsorption spectroscopy as a tool for probing charge transfer and state mixing in thermally activated delayed fluorescence emitters. J Phys Chem Lett 2019;10(12):3205–11.
[39] Etherington MK, Gibson J, Higginbotham HF, Penfold TJ, Monkman AP. Revealing the spin-vibronic coupling mechanism of thermally activated delayed fluorescence. Nat Commun 2016;7:13680.
[40] Gibson J, Monkman AP, Penfold TJ. The importance of vibronic coupling for efficient reverse intersystem crossing in thermally activated delayed fluorescence molecules. ChemPhysChem 2016;17(19):2956–61.
[41] Penfold TJ, Gindensperger E, Daniel C, Marian CM. Spin-vibronic mechanism for intersystem crossing. Chem Rev 2018;118(15):6975–7025.
[42] Yao H, Ye L, Zhang H, Li S, Zhang S, Hou J. Molecular design of benzodithiophene-based organic photovoltaic materials. Chem Rev 2016;116(12):7397–457.
[43] Zheng B, Huo L, Li Y. Benzodithiophenedione-based polymers: recent advances in organic photovoltaics. NPG Asia Mater 2020;12(1):3.
[44] Dos Santos PL, Ward JS, Bryce MR, Monkman AP. Using guest-host interactions to optimize the efficiency of TADF OLEDs. J Phys Chem Lett 2016;7(17):3341–6.
[45] Lee I, Lee JY. Molecular design of deep blue fluorescent emitters with 20% external quantum efficiency and narrow emission spectrum. Org Electron 2016;29:160–4.
[46] Haase N, Danos A, Pflumm C, Morherr A, Stachelek P, Mekic A, et al. Kinetic modeling of transient photoluminescence from thermally activated delayed fluorescence. J Phys Chem C 2018;122(51):29173–9.
[47] Furue R, Matsuo K, Ashikari Y, Ooka H, Amanokura N, Yasuda T. Highly efficient red-orange delayed fluorescence emitters based on strong π-accepting dibenzophenazine and dibenzoquinoxaline cores: toward a rational pure-red OLED design. Advanced Optical Materials 2018;6(5).
[48] Cardeynaels T, Paredis S, Deckers J, Brebels S, Vanderzande D, Maes W, et al. Finding the optimal exchange-correlation functional to describe the excited state properties of push-pull organic dyes designed for thermally activated delayed fluorescence. Phys Chem Chem Phys 2020;22(28):16387–99.
[49] Penfold TJ. On predicting the excited-state properties of thermally activated delayed fluorescence emitters. J Phys Chem C 2015;119(24):13535–44.
[50] Frisch Gwt MJ, Schlegel HB, Scuseria GE, Robb MA, Cheeseman JR, Scalmani G, Barone V, Petersson GA, Nakatsuji H, Li X, Caricato M, Marenich AV, Bloino J, Janesko BG, Gomperts R, Mennucci B, Hratchian HP, Ortiz JV, Izmaylov AF, Sonnenberg JL, Williams-Young D, Ding F, Lipparini F, Egidi F, Goings J, Peng B, Petrone A, Henderson T, Ranasinghe D, Zakrzewski VG, Gao J, Rega N, Zheng G, Liang W, Hada M, Ehara M, Toyota K, Fukuda R, Hasegawa J, Ishida M, Nakajima T, Honda Y, Kitao O, Nakai H, Vreven T, Throssell K, Montgomery Jr JA, Peralta JE, Ogliaro F, Bearpark MJ, Heyd JJ, Brothers EN, Kudin KN, Staroverov VN, Keith TA, Kobayashi R, Normand J, Raghavachari K, Rendell AP, Burant JC, Iyengar SS, Tomasi J, Cossi M, Millam JM, Klene M, Adamo C, Cammi R, Ochterski JW, Martin RL, Morokuma K, Farkas O, Foresman JB, Fox DJ. Gaussian 16, revision A.03. Wallingford CT: Gaussian, Inc.; 2016.
[51] Le Bahers T, Adamo C, Ciofini I. A qualitative index of spatial extent in charge-transfer excitations. J Chem Theor Comput 2011;7(8):2498–506.
[52] Ward JS, Danos A, Stachelek P, Fox MA, Batsanov AS, Monkman AP, et al. Exploiting trifluoromethyl substituents for tuning orbital character of singlet and triplet states to increase the rate of thermally activated delayed fluorescence. Materials Chemistry Frontiers 2020;4:3602–15. https://doi.org/10.1039/D0QM00429D.
[53] Wang S, Cheng Z, Song X, Yan X, Ye K, Liu Y, et al. Highly efficient long-wavelength thermally activated delayed fluorescence OLEDs based on dicyanopyrazino phenanthrene derivatives. ACS Appl Mater Interfaces 2017;9(11):9892–901.
[54] Aksoy E, Danos A, Varlikli C, Monkman AP. Navigating CIE space for efficient TADF downconversion WOLEDs. Dyes Pigments 2020:108707.
[55] Crucho CIC, Avó J, Nobuyasu R, Pinto S N, Fernandes F, Lima JC, et al. Silica nanoparticles with thermally activated delayed fluorescence for live cell imaging. Mater Sci Eng C 2020;109:110528.
[56] Xiong X, Song F, Wang J, Zhang Y, Xue Y, Sun L, et al. Thermally activated delayed fluorescence of fluorescein derivative for time-resolved and confocal fluorescence imaging. J Am Chem Soc 2014;136(27):9590–7.
[57] Wu Y, Jiao L, Song F, Chen M, Liu D, Yang W, et al. Achieving long-lived thermally activated delayed fluorescence in the atmospheric aqueous environment by nano-encapsulation. Chem Commun 2019;55(96):14522–5.